Phys Chem Minerals (2007) 34:599–607
DOI 10.1007/s00269-007-0174-6

ORIGINAL PAPER

Dauphiné twinning and texture memory in polycrystalline quartz

Part 2: In situ neutron diffraction compression experiments

H.-R. Wenk · M. Bortolotti · N. Barton · E. Oliver · D. Brown

Received: 14 March 2007 / Accepted: 21 June 2007 / Published online: 22 August 2007

Abstract Mechanical twinning in polycrystalline quartz was investigated in situ with time-of-flight neutron diffraction and a strain diffractometer. Dauphiné twinning is highly temperature sensitive. It initiates at a macroscopic differential stress of 50–100 MPa and, at 500°C, saturates at 400 MPa. From normalized diffraction intensities the patterns of preferred orientation (or texture) can be inferred. They indicate a partial reversal of twinning during unloading. The remaining twins impose residual stresses corresponding to elastic strains of 300–400 microstrain. Progressive twinning on loading and reversal during unloading, as well as the temperature dependence, can be reproduced with finite element model simulations.

Keywords Quartz · Mechanical twinning · In situ neutron diffraction · FEM

H.-R.Wenk (✉) · M. Bortolotti
Department of Earth and Planetary Science,
University of California, Berkeley, CA 94720, USA
e-mail: wenk@seismo.berkeley.edu

N. Barton
Lawrence Livermore National Laboratory,
Livermore, CA 94551, USA

E. Oliver
ISIS, Rutherford Appleton Laboratory,
Chilton, Didcot OX11 0QX, UK

D. Brown
Lujan Center, Los Alamos National Laboratory,
Los Alamos, NM 87545, USA

Introduction

In a previous study we have investigated the role of mechanical Dauphiné twinning in polycrystalline quartz (Wenk et al. 2006). We revisited Dauphiné twinning in fine-grained quartz aggregates (Tullis and Tullis 1972) with a state-of-the-art deformation apparatus to quantify the role of stress and temperature. It was observed that the activity of twinning is highly dependent on temperature and initiates at about 100 MPa at 500°C. Mechanical twinning in an aggregate is expressed in the pattern of preferred orientation or texture (we use the term texture here, which is universally accepted in materials science and there should be no confusion with the different meaning of "petrographic texture". Lattice preferred orientation (LPO) should not be used for quartz where the hexagonal lattice does not describe the trigonal symmetry of the crystal structure).

In the course of these previous investigations a number of issues emerged that could not be resolved: does the texture produced in a compression experiment and then measured ex situ represent the true twinning pattern that was produced by stressing or does part of twinning revert upon unloading? Does the twinning pattern change with time as a stress is applied or does it stabilize very quickly? What is the threshold stress at different temperatures? And how is the twinning pattern influenced if a stress is applied during the phase transformation? All these questions could best be resolved with in situ experiments, i.e. observing changes in twinning as stress is applied to the sample. Such experiments are indeed possible with neutron diffraction and strain diffractometers, where a stress is applied to the sample and changes in twinning patterns are observed through changes in diffraction intensities. Analogous experiments have been performed on hexagonal metals that

display mechanical twinning (Agnew and Duygulu 2005; Brown et al. 2003). This describes a first application of this technique to rocks. In quartz the situation is simplified, because at the conditions of the experiments, deformation occurs solely by twinning, with no activity of dislocation glide.

Experimental

Time-of-flight (TOF) neutron diffraction has become a favorite technique to investigate in situ structural changes and internal stresses during deformation (Daymond 2006). Another method is synchrotron X-ray diffraction (Fitzpatrick and Lodini 2003). Here we use two engineering diffractometers, SMARTS at the Lujan Center of Los Alamos National Laboratory and ENGIN-X at ISIS of the Rutherford Appleton Laboratory. Both are equipped with a press and two detector panels at $2\theta = 90°$ to the incident neutron beam. The press is positioned at 45° so that one panel ($2\theta = +90°$) records lattice planes that are perpendicular to the compression direction and the other panel ($2\theta = -90°$) records lattice planes that are parallel to the compression direction (Fig. 1). The diffractometer is equipped with a radiant heater. For details of the instruments we refer to the literature (SMARTS: Brown et al. 2003, http://www.lansce.lanl.gov/lujan/instruments/SMARTS/pdfs/SMARTS.pdf; ENGIN-X: Johnson and Daymond 2002; Santisteban et al. 2006, http://www.isis.rl.ac.uk/engineering/).

The samples are cylinders, 2 cm in length and 1 cm in diameter, of a fine-grained (10 μm), dense and homogeneous quartz aggregate (novaculite) from Arkansas. It is similar to the material used in the previous study (Wenk et al. 2006) and has initially no preferred orientation.

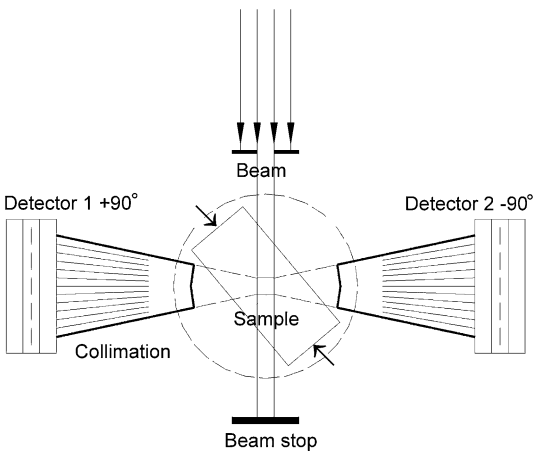

Fig. 1 Schematic of a TOF neutron stress diffractometer

Samples were investigated at different temperature–stress conditions and details are summarized in Table 1. In the first experiments differential stress was increased from 0 to 500 MPa, while recording diffraction patterns at regular stress intervals. In the last experiment stress was increased in a few steps, with many recordings at the same stress level. After reaching the maximum stress level, stress was lowered, recording changes during unloading. A pair of TOF diffraction spectra from the two detectors is shown in Fig. 2a, b for a sample compressed to 500 MPa at 500°C. These spectra are corrected for incident beam intensity and intensities are expressed as function of TOF (in ms). The TOF is directly proportional to the *d*-spacing (TOF = d ($2mL\sin\theta/h$), where m is the mass of the neutron, L the flight path and h Planck's constant). Note that relative intensities of some diffraction peaks in the two spectra are different and this is due to preferred orientation of crystallites and thus mechanical twinning. For example the intensity of the $20\bar{2}1$ diffraction peak is three times that of the $20\bar{2}0$ diffraction peak for the +90° detector (lattice planes perpendicular to compression, Fig. 2a) and less than two times for the –90° detector (Fig. 2b). For the +90° detector $11\bar{2}2$ is smaller than $10\bar{1}2 + 01\bar{1}2$ while the reverse is true for the –90° detector.

Data analysis

Integrated intensities and positions of selected diffraction peaks were obtained by fitting the intensity profiles with TOF profile function 3 as defined in the GSAS manual (Larson and Von Dreele 2004, p. 147), using the rawplot routine in the software package GSAS. A typical fit is shown in Fig. 3. Standard deviations for peak positions are about 10^{-5} Å and for intensities about 1% of the raw value. Intensities of some reflections change systematically during compression. To study these changes quantitatively, intensities need to be normalized since the neutron flux is not constant over time. Some reflections (*hkil*, Miller–Bravais indices) are not affected by Dauphiné twinning, such as prisms and basal lattice planes. Other reflections are sensitive to twinning, specifically rhombohedral lattice planes $\{h0\bar{h}l\}$. We chose to normalize all reflections to the

Table 1 Information about experiments

Sample number	Instrument	Stress range (MPa)	Temperature (°C)
N 1-1	SMARTS	0–500	500
N 1-2	ENGIN-X	0–500	400
N 1-3	ENGIN-X	0–500	300
N 1-10	SMARTS	0–300	500

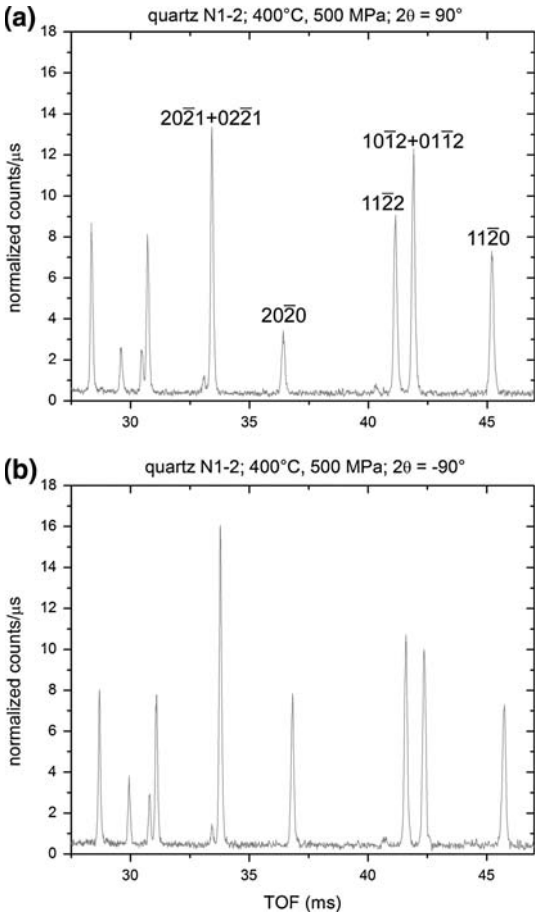

Fig. 2 Two diffraction spectra for N1-2, 400°C, 500 MPa. **a** +90° detector, **b** –90° detector (ENGIN-X)

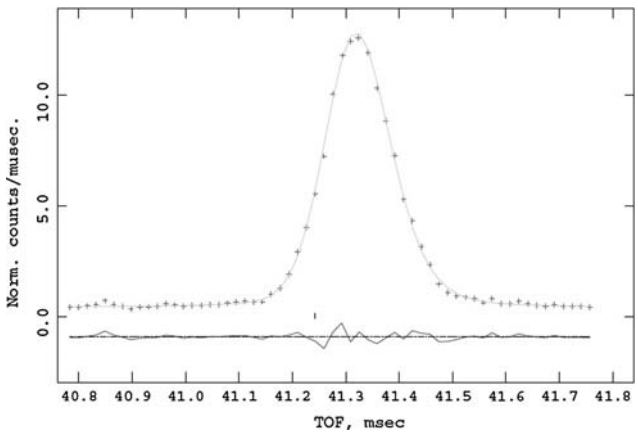

Fig. 3 Typical peak fit with GSAS of the $20\bar{2}1 + 02\bar{2}1$ reflection. *Crosses* are data and *line* is fit. Deviation is illustrated below

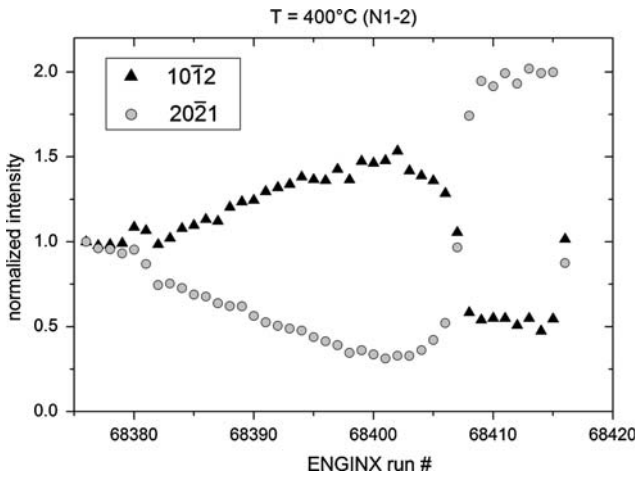

Fig. 4 Sequence of experiments. Normalized intensity versus run number for N1-2 (ENGIN-X, increasing stress to 500 MPa from 68376 to 68402, then unloading from 68403 to 68406 at 400°C, and finally a heating cycle at 10 MPa through the α–β phase transformation, from 68407 to 68417)

strong diffraction peak $11\bar{2}0$ that is insensitive to twinning and we used mainly the two rhombohedral reflections $10\bar{1}2$ and $20\bar{2}1$ to follow activation of Dauphiné twinning. Figure 4 illustrates these normalized intensity changes for sample N1–2 that was first compressed at 400°C to 500 MPa (from run # 68376 to 68402 at ENGIN-X), and then the stress was reversed to 0 MPa (from # 68403 to 68406) and finally the sample was cycled through the trigonal–hexagonal phase transformation by heating to 630°C and cooling back to 400°C at a constant stress of 10 MPa (from 68407 to 68417). Intensities for $20\bar{2}1$ decrease during compression, reverse somewhat during unloading, become very strong after the phase transformation and, after thermal cycling, return to the original value. For $10\bar{1}2$ the relative intensity changes are just the opposite. The intensity changes with stress at constant temperature (400°C) can be attributed to mechanical twinning. Intensity changes with heating and cooling are due to changes in crystal structure.

Intensities for positive $\{h0\bar{h}l\}$ and negative rhombs ($\{0h\bar{h}l\}$ for trigonal quartz are different, even though the lattice planes have identical d-spacings and are thus superposed in the diffraction pattern. Positive and negative rhombs are related by a 180° rotation around the c axis and thus good indicators for mechanical Dauphiné twinning. Negative rhombs have a large Young's modulus (the maximum is close to $02\bar{2}1$) and positive rhombs a small one (with a minimum close to $20\bar{2}1$; Ohno et al. 2006). Thus, to minimize elastic strain energy, in compression twinning switches orientations with negative rhombs perpendicular to the compression direction to positive rhombs perpendicular to the compression direction (Tullis and Tullis 1972). For some reflections the positive rhomb has a higher intensity contribution $(10\bar{1}2)$, for others it is weaker $(20\bar{2}1)$. Since twinning favors positive rhombs perpendicular to the compression direction, the former are expected

to get stronger and the latter to get weaker during compression, and this seems to be qualitatively the case (Fig. 4).

The structure of quartz has been refined at different temperatures and there are significant changes (Kihara 1990): with increasing temperature the positions of oxygen approach continuously those in the hexagonal configuration and anisotropic thermal vibrations change greatly (Fig. 5). These structural changes cause significant changes in diffraction intensities, including relative contributions of rhombohedral reflections to superposed diffraction peaks (Fig. 6). Thus, for a quantitative interpretation of diffraction spectra, these structural changes have to be taken into account. Note that in this study we use space group $p3_121$ where $r = 10\bar{1}1$ is the morphological dominant rhomb with high diffraction intensity (both for neutrons and X-rays) and a low stiffness. In the literature there are some discrepancies about this issue (see Heaney 1994, p. 8).

An elegant way to obtain quantitative texture information from TOF diffraction spectra is the Rietveld method. It generally relies on multidetector diffractometers and measurements in various sample orientations (Wenk et al. 2003; Matthies et al. 2005). In the present study there are only two detectors and the sample can not be rotated. A Rietveld refinement with the software MAUD (Lutterotti et al. 1999) of the sample N1-1 at 500 MPa and 500°C was nevertheless successful. The crystal structure at the correct temperature was imposed. The refinement used the two detectors and a *d*-range 1.0–2.7 A, the discrete texture algorithm EWIMV imposing axial symmetry, and orientation space cells of 15°. Clearly using only two detectors is not optimal but even with these minimal experimental data the inverse pole figure (Fig. 7a) compares satisfactorily with that obtained in ex situ experiments at similar conditions (Fig. 7b; Wenk et al. 2006). Assuming an initial random orientation distribution and only reorientation by twinning, a pole density maximum of two multiples of a random distribution (mrd) for positive rhombs near $20\bar{2}1$ indicates that all these orientations have twinned, with a value of close to zero mrd for corresponding negative rhombs. The Rietveld procedure is very complex and it is impractical to analyze the many data sets recorded. For the routine analysis we will rely on normalized integrated peak intensities of reflections $10\bar{1}2$ and $20\bar{2}1$. Notice in Fig. 7 that $20\bar{2}1$ is close to the texture minimum and $02\bar{2}1$ close to the texture maximum in the inverse pole figure, corresponding to maximum and minimum Youngs modulus, respectively. $10\bar{1}2$ is closer to the *c* axis and less susceptible to twinning.

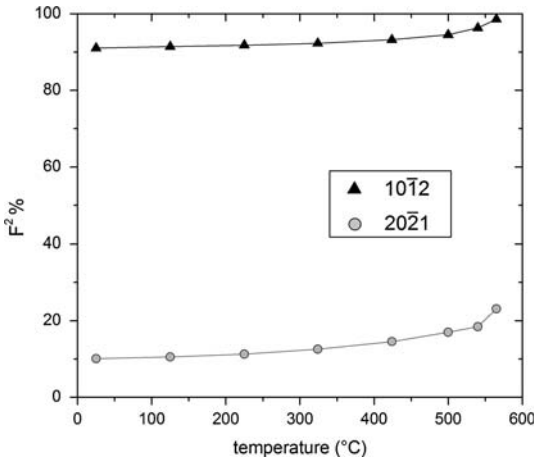

Fig. 6 Changes in relative intensity for positive rhombs $10\bar{1}2$ and $20\bar{2}1$ with temperature. These relative changes are used for the texture analysis

The relative intensity variations, normalized to $11\bar{2}0$ indicate a systematic trend of texture changes relative to loading (Fig. 4) but for a quantitative assessment of texture we need to take the crystal structure into account. Again, we assume that the initial orientation distribution is random (1 mrd). During compression the only orientation changes occur through twinning with no crystal plasticity by slip. Thus orientations at negative rhombs are depleted and orientations at positive rhombs are correspondingly enhanced. For the peak intensity we can write the following equation:

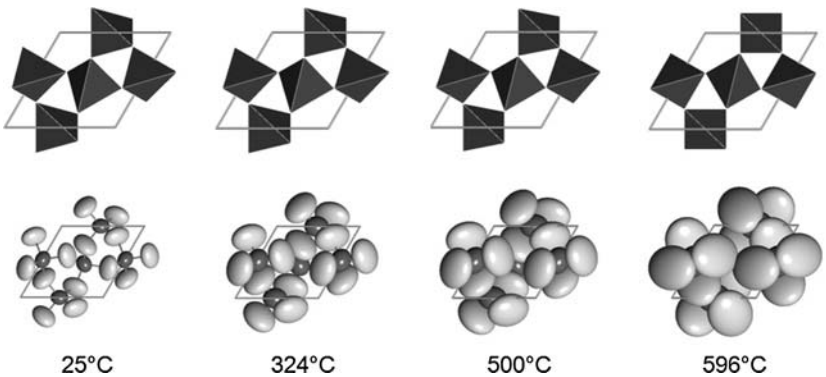

Fig. 5 Changes in quartz structure with temperature. *Top* oxygen positions displayed as [SiO_4] tetrahedra. *Bottom* thermal vibration (99% probability surface). Structural data from Kihara (1990), plots generated with XtalDraw

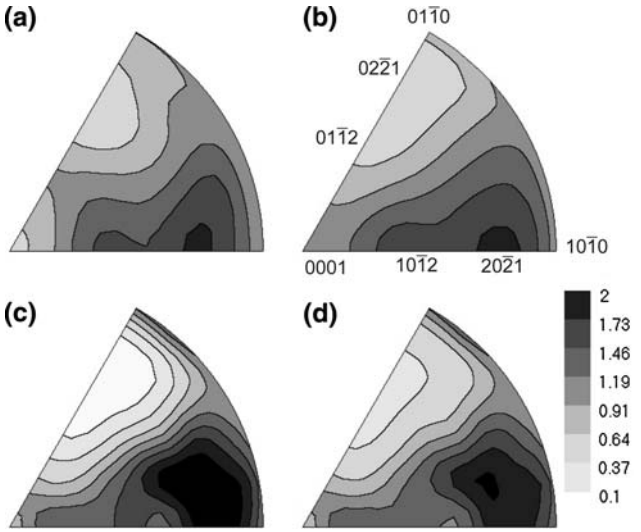

Fig. 7 Inverse pole figures. **a** In situ N1-1, 500 MPa, **b** ex situ (N2-5 from Wenk et al. 2006), **c**, **d** results of FEM simulations at 500°C and 500 MPa. **c** is after maximum load and **d** after unloading. Equal area projection, linear scale in multiples of a random distribution

$$I = N\{(1+m)F_{h0l}^2 + (1-m)F_{0hl}^2\}$$

where N is a normalization factor, F_{h0l} and F_{0hl} are structure factors for positive and negative rhombs (based on the Kihara's 1990 structure), respectively, and m is the normalized texture measure (in mrd). From this m we can solve for the pole density $(1 + m)$. The pole density for random is 1 mrd; it can not be larger than 2 mrd and can not be less than 0. These $(m + 1)$ values for positive rhombs 10$\bar{1}$2 and 20$\bar{2}$1 (in mrd) will be used for the analysis.

Results

Figure 8 illustrates texture evolution for the two positive rhombs with stress for three different temperatures. Let us first look at the 500°C data. Here twinning initiates at about 50 MPa and progresses with increasing stress, saturating for 20$\bar{2}$1 around 500 MPa at 2 mrd. Thus these orientations are completely twinned. For 10$\bar{1}$2 twinning is less effective and saturates at 1.75 mrd. Upon unloading some twinning is reversed to 1.7 mrd for both directions (Fig. 8c). At 400°C the results are similar, though 10$\bar{1}$2 never exceeds 1.5 mrd (Fig. 8b). At 300°C twinning is highly reduced, reaching only 1.6 mrd for 20$\bar{2}$1 and 1.25 mrd for 10$\bar{1}$2 (Fig. 8a). There is not much reversal upon unloading.

In the previous experiments stress was increased continuously over 12 h with only one measurement at each stress level. In order to assess the influence of time on twinning we conducted a SMARTS experiment with

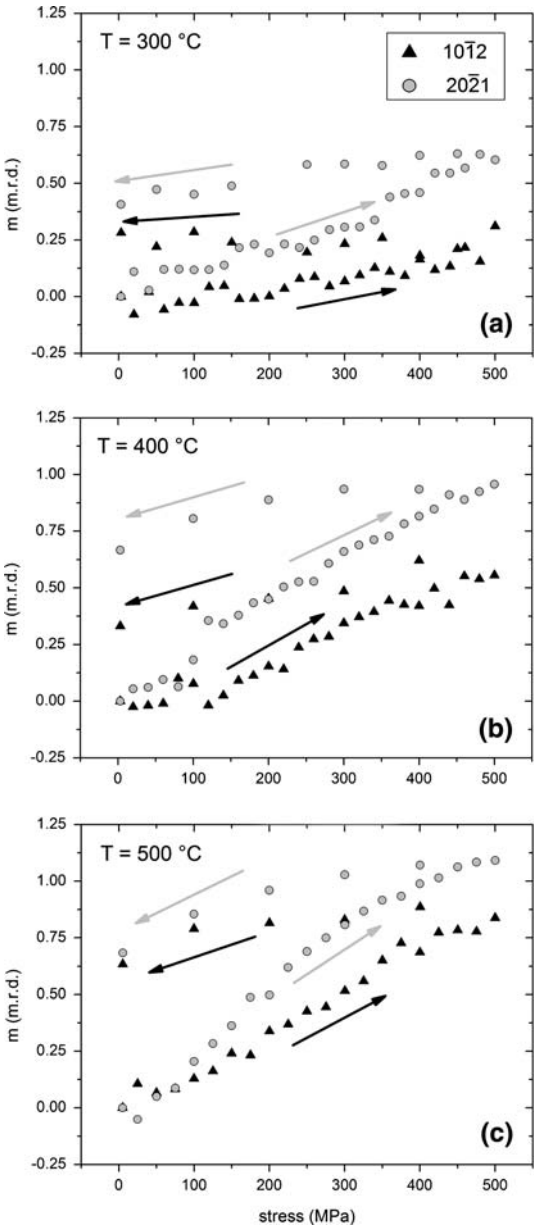

Fig. 8 Pole densities indicative of mechanical twinning for 10$\bar{1}$2 and 20$\bar{2}$1 parallel to the compression direction (in m.r.d.) versus stress for 300, 400 and 500°C; 1 mrd is random and 2 mrd is completely twinned. *Arrows* indicate the changes with loading and unloading, respectively

stepwise stress increase with experiments extending over 20 h (SMARTS run # 35983–36015; Fig. 9). This experiment was hampered by various interferences. The neutron beam was off for extended periods. The stress level calculated from the applied force seems to be erroneous because neither pole densities (from intensity changes) nor lattice strains correspond to those observed previously at the same conditions. We suspect that actual stresses were about one-third of the indicated values. Thus we used

lattice strains to infer stresses in Fig. 9. Intensity changes for $10\bar{1}2$ and $20\bar{2}1$ follow the stress steps, indicating that the twin activation is fast compared with the duration of an experiment.

The experiment N1-2 passed through the trigonal–hexagonal phase transformation at 10 MPa stress (Fig. 4). In hexagonal β-quartz there is no Dauphiné twinning. After thermal cycling the material returns to the random starting texture rather than the texture pattern imposed during the compression cycle. In other words there is no texture memory. We will report on this memory effect and variant selection between the two trigonal orientation variants in a future paper.

So far we discussed diffraction intensity changes and their relationship to twinning. From changes in peak positions we can evaluate lattice strains, i.e. the difference between the initial d-spacing and the deformed lattice spacing (elastic lattice strains are defined using the initial value at the beginning of the experiment (d^0_{hkl}) as reference: $\varepsilon_{hkl} = \frac{d_{hkl}}{d^0_{hkl}} - 1$ and usually expressed as microstrains $\varepsilon \times 10^6$; see SMARTS SPF manual). Results for both detectors are shown in Fig. 10 for 500°C. In the compression direction lattice spacings decrease in an almost linear fashion and this is more or less reversible upon unloading (Fig. 10a). Details will be discussed below. More surprisingly, perpendicular to the compression direction, lattice spacings also decrease, though much less and also non-linearly (Fig. 10b). This is due to a very small and even negative Poisson's ratio for α-quartz at higher temperature (Ohno et al. 2006). At higher stresses lattice strains increase again.

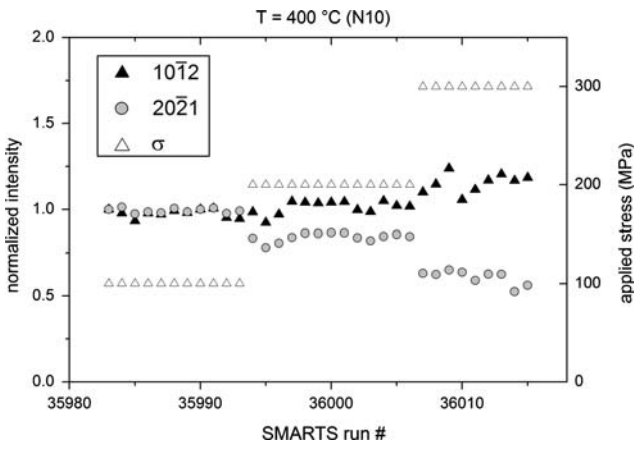

Fig. 9 Texture changes expressed in intensity changes of rhombohedral reflections with stepwise stress increase. The stress is calculated from lattice strain because of problems with SMARTS force gauge. Note that intensity change follows the stress steps

Discussion

In situ neutron diffraction experiments with a strain diffractometer establish that mechanical twinning starts at 50–100 MPa and is expressed in systematic intensity changes in diffraction patterns that can be converted to quantitative texture changes (Fig. 8). Clearly twinning is strongly temperature dependent, consistent with ex situ experiments (Wenk et al. 2006). Some twinning reverts when stress is released and thus ex situ experiments may not convey the full picture. The amount of reversal is highest at high temperature and for orientations optimally oriented for twinning (about 30% of the twinning reverts at 500°C).

The twinning pattern is not maintained when novaculite is heated above the phase transformation and cooled. In this case the orientation distribution becomes random

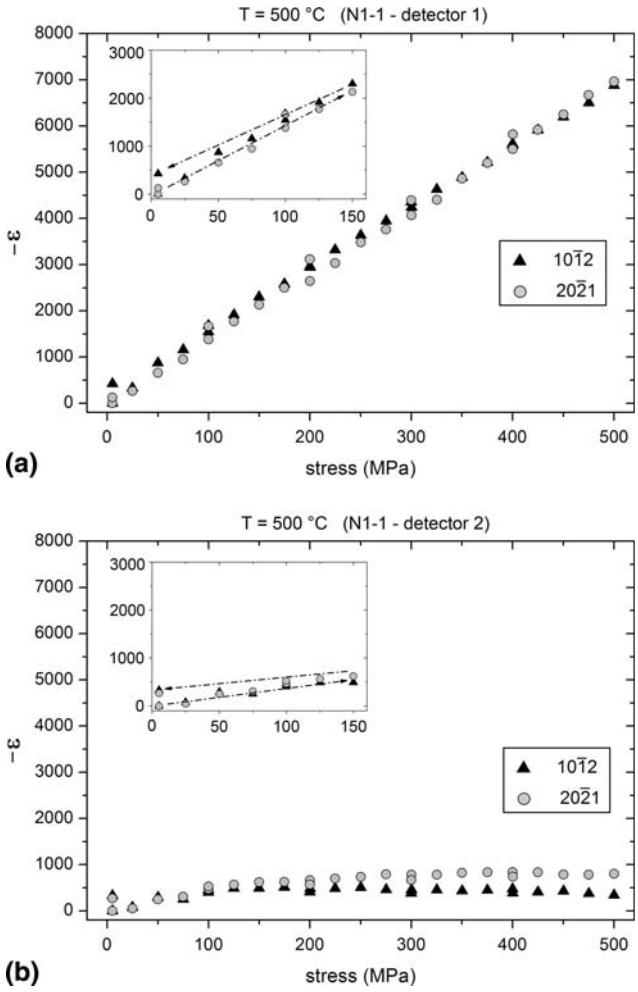

Fig. 10 Lattice strain (in microstrain units) versus stress. **a** +90° detector, **b** –90° detector for sample N1-1, 500°C. The inset is an enlarged portion of the low stress region that illustrates a small but significant microstrain after unloading. *Arrows* indicate loading/unloading, respectively (compare with Fig. 8c)

again. This is different from naturally deformed quartz rocks where a perfect texture memory with respect to Dauphiné twins is documented by in situ neutron diffraction experiments (Wenk 2006).

Lattice strains after cycling are somewhat higher than initially which is best seen in the inset to Fig. 10 and suggests that some residual stress is maintained after unloading. The strains (about 200–300 microstrains) are very small and at the limit of the resolution of TOF strain diffractometers (standard deviations of microstrains are about 1% for ENGIN-X and 2% for SMARTS). First we thought it was a random deviation but it was consistent in all three experiments, suggesting that it is real. The strains are slightly higher at higher temperature, corresponding to more twinning.

In order to better understand the complex observations we have used a finite element model to investigate twinning in quartz. We make use of a material model that treats phase and twinning transformations which has been developed for the α–ε transformation in iron (Barton et al. 2005). In this model, each material element is made up of microstructural constituents, with each constituent having its own mass fraction. Stress and temperature equilibrium are assumed among the constituents. For the application to quartz, the microstructure is composed of three constituents, with transformation paths between each of them: α-quartz in host orientation, α-quartz in twin orientation and β-quartz. Transformation is used as a generic term for either a twinning transformation or a phase change transformation. Each constituent has its own lattice orientation, with anisotropic properties oriented with respect to that lattice. For quartz the elastic anisotropy is of primary concern. The kinetics for twinning employ an activation energy which decreases as the temperature approaches the phase transformation temperature, motivated by computed potential energy curves (Smirnov and Mirgorodsky 1997; Kimizuka et al. 2003) as well as experimental observations of extensive small scale twinning near the transformation temperature (Sorrell et al. 1974). The most salient features of the formulation for quartz are described below and further details may be found elsewhere (Barton and Wenk 2007).

In the special case of twinning transformations, the driving force takes the form

$$f = \boldsymbol{\tau}\text{:symm}(\ln(\boldsymbol{V}_{\text{to}} \cdot (\boldsymbol{V}_{\text{fr}})^{-1}))$$

with $\boldsymbol{\tau}$ being a measure of stress and $\boldsymbol{V}_{\text{to}}$ and $\boldsymbol{V}_{\text{fr}}$ being the thermo-elastic lattice strains in the product and parent α variants, respectively. Differential anisotropic thermo-elastic stretch of the trigonal structures therefore controls the driving force for twinning. While increases in temperature soften the twinning kinetics, they also decrease the driving force due to decreases in elastic anisotropy with temperature.

Material parameters used in the simulations are obtained from a variety of sources. Elasticity data are approximated from Ohno (1995). Lattice parameters and thermal expansion data are drawn from Kihara (1990).

Figure 11 shows computed pole figure values for $20\bar{2}1$ and $10\bar{1}2$ in the compression direction from finite element simulations of compression at 500°C. Aggregates in the polycrystal initially contain 512 grains with random orientation, each discretized by $4 \times 4 \times 4$ finite elements. Model predictions give reasonable agreement with experimental results, including the overall degree of twinning and the partial reversal of twinning upon unloading (compare with Fig. 8c).

Figure 12 illustrates the computational domains with gray shades illustrating amount of mechanical twinning. It is assumed that initially no twinning is present and the grains are stress-free at ambient temperature. After heating to 500°C (Fig. 12a) and straining in compression, orientations that are favorable for twinning twin (Fig. 12b). A corresponding inverse pole figure is shown in Fig. 7c and compares well with the experiment (Fig. 7a, b), i.e. orientations near $20\bar{2}1$ are completely twinned (pole densities at $02\bar{2}1$ are zero and at $20\bar{2}1$ near 2.0 mrd) and those near $10\bar{1}2$ are partially twinned. Notice that with only 512 grains orientation statistics are limited and minor deviations are artifacts. Upon unloading some twinning reverses (Figs. 12c, 7d), again consistent with experiments. Note that similar simulations conducted using a uniform deformation assumption (such as Taylor) instead of the finite element method do not predict reversal. This indicates that

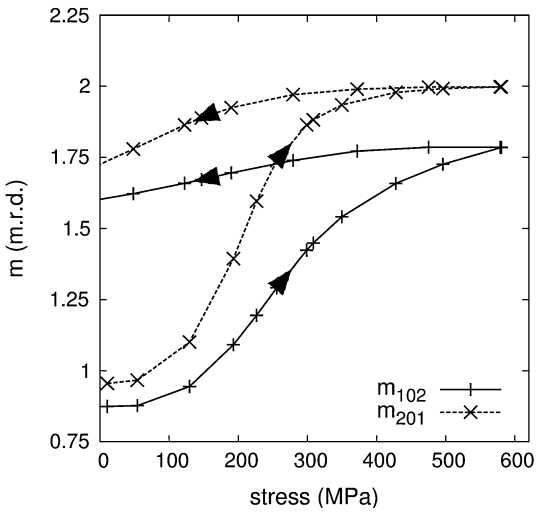

Fig. 11 Simulations of maximum pole densities (in mrd) of lattice planes $10\bar{1}2$ and $20\bar{2}1$ perpendicular to the compression direction, versus stress at 500°C. Compare with Fig. 8c

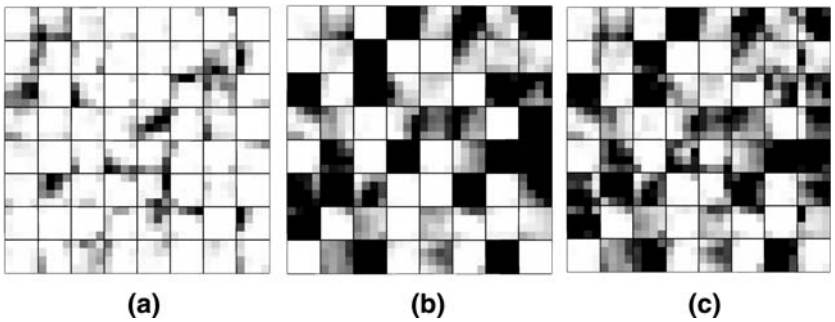

Fig. 12 Finite element simulations of mechanical twinning in quartz, with 8-by-8-by-8 grains whose initial orientations are drawn from a uniform texture. *Plots* show data on slices through the interior of the idealized microstructure. Twinned domains are indicated with *gray shades* (*black* completely twinned). **a** structure at 500°C (minor twinning induced by thermal stresses); **b** loaded to 580 MPa at 500°C, **c** unloaded at 500°C (some twinning is reversed). Textures for **b** and **c** are shown in Fig. 7c, d respectively

reversal of twinning is significantly influenced by interactions of grains through the stress field.

A difference in orientation of positive and negative rhombs is widely observed in quartz-bearing rocks (e.g. Pehl and Wenk 2005). It may be the result of so far undocumented rhombohedral slip systems, but more likely it is an effect of mechanical twinning. The new experiments support this conclusion, particularly at higher temperatures as obtained in metamorphic rocks. In those the orientation pattern can then be interpreted in terms of paleostresses. Twinning occurs rapidly and thus is found in shocked quartzites during meteorite impacts (Trepmann and Spray 2005) where it changes the texture pattern (Wenk et al. 2005). Mechanical twinning in perovskites has been shown to be time-dependent but on a scale of microseconds and saturating after that (Harrison et al. 2003).

In this study we have investigated the effect of temperature, stress and time. In the future one should determine the effect of microstructure, particularly grain size. If analogy to carbonates (Barber and Wenk 1979) and metals (El-Danaf et al. 1999) holds, twinning should be more easily activated in coarse-grained materials than in fine-grained novaculites.

Conclusions

The in situ straining experiments establish that Dauphiné twinning occurs rapidly on the time scale of the experiments and stabilizes within minutes. As observed previously twinning is highly temperature and orientation dependent. Contrary to previous studies that assumed that ex situ texture determinations represent twinning patterns attained in the deformation experiments, the new investigation shows that a substantial amount of twinning reverses upon unloading. Activation of twinning during compression, the orientation dependence and the twin reversal are all well captured using the finite element method in conjunction with a crystal level material model. Thus the model can be used to understand experimentally observed behaviors and, perhaps after further calibration, to predict behaviors under other thermo-mechanical loading scenarios.

Acknowledgments We are appreciative to Erik Rybacki for providing novaculite samples. In situ deformation measurements were performed with neutron diffraction at LANSCE (SMARTS) and ISIS (ENGIN-X). Comments from C. McCammon, J. Tullis and an anonymous reviewer were very helpful. Research was supported by NSF (EAR 0337006), DOE (DE-FG02-05ER15637) and IGPP-LLNL. The work of NB was performed under the auspices of the U.S. Department of Energy by University of California, Lawrence Livermore National Laboratory under Contract W-7405-Eng-48 (UCRL-JRNL-227703).

References

Agnew SR, Duygulu O (2005) Plastic anisotropy and the role of non-basal slip in magnesium alloy AZ31B. Int J Plast 21:1161–1193

Barber DJ, Wenk H-R (1979) Deformation twinning in calcite, dolomite, and other rhombohedral carbonates. Phys Chem Miner 5:141–165

Barton NR, Wenk H-R (2007) Dauphiné twinning in polycrystalline quartz. Modell Simul Mater Sci Eng (in press)

Barton NR, Benson DJ, Becker R (2005) Crystal level continuum modelling of phase transformations: the $\alpha \leftrightarrow \varepsilon$ transformation in iron. Modell Simul Mater Sci Eng 13:707–731

Brown DW, Bourke MAM, Clausen B, Holden TM, Tome CN, Varma R (2003) A neutron diffraction and modeling study of uniaxial deformation of polycrystalline beryllium. Met Mater Trans A 34A:1439–1449

Daymond MR (2006) Internal stresses in deformed crystal aggregates. In: Wenk HR (ed) Neutron Scattering in Earth Sciences. Rev Miner Geochem 63:427–458

El-Danaf E, Kalindi SR, Doherty RD (1999) Influence of grain size and stacking fault energy on deformation twinning in Fcc metals. Metall Mater Trans A30:1223–1233

Fitzpatrick ME, Lodini A (eds) (2003) Analysis of residual stress by diffraction using neutron and synchrotron radiation. Taylor & Francis, London, p 354

Harrison RJ, Redfern SAT, Buckley A, Salje EKH (2003) Application of real-time, stroboscopic x-ray diffraction with dynamical mechanical analysis to characterize the motion of ferroelastic domains. J Appl Phys 95:1706–1717

Heaney PJ (1994) Structure and chemistry of the low pressure silica polymorphs. In: Heaney PJ, Prewitt CT, Gibbs GV (eds) Silica. Physical behavior, geochemistry and materials applications, Chap 1. Rev Mineral 29:1–32

Johnson MW, Daymond MR (2002) An optimum design for a time-of-flight neutron diffractometer for measuring engineering stresses. J Appl Cryst 35:49–57

Kihara K (1990) An X-ray study of the temperature dependence of the quartz structure. Eur J Mineral 2:63–77

Kimizuka H, Kaburaki H, Kogure Y (2003) Molecular-dynamics study of the high-temperature elasticity of quartz above the α–β phase transition. Phys Rev B 67:024105

Larson AC, Von Dreele RB (2004) General structure analysis system (GSAS). Los Alamos Natl Lab Rep LAUR 86–748

Lutterotti L, Matthies S, Wenk H-R (1999) MAUD: a friendly Java program for materials analysis using diffraction. Int Union Crystallogr Comm Powder Diffraction Newsl 21:14–15

Matthies S, Pehl J, Wenk H-R, Vogel S (2005). Quantitative texture analysis with the HIPPO TOF diffractometer. J Appl Cryst 38:462–475

Ohno I (1995) Temperature variation of elastic properties of α-quartz up to the α–β transition. J Phys Earth 43:157–169

Ohno I, Harada K, Yoshitomi C (2006) Temperature variation of elastic constants of quartz across the α–β transition. Phys Chem Minerals 33:1–9

Pehl J, Wenk H-R (2005) Evidence for regional Dauphiné twinning in quartz from the Santa Rosa mylonite zone in Southern California. A neutron diffraction study. J Struct Geol 27:1741–1749

Santisteban JR, Daymond MR, James JA, Edwards L (2006) ENGIN-X: a third generation neutron strain scanner. J Appl Cryst 39:812–825

Smirnov MB, Mirgorodsky AP (1997) Lattice-dynamical study of the α–β phase transition of quartz: soft-mode behavior and elastic anomalies. Physical Review Letters 78:2413–2416

Sorrell AC, Anderson HU, Ackermann RJ (1974) Thermal expansion and the high-low transformation in quartz. II. Dilatometric studies. J Appl Cryst 7:468–473

Trepmann CA, Spray JG (2005) Planar microstructures and Dauphiné twins in shocked quartz from the Charlevoix impact structure, Canada. Geol Soc Am Spec Pap 384:315–328

Tullis J, Tullis TE (1972) Preferred orientation produced by mechanical Dauphiné twinning. Thermodynamics and axial experiments. Am Geophys Union Monogr 16:67–82

Wenk H-R (2006) Neutron diffraction texture analysis. In Neutron Scattering in Earth Sciences. Reviews in Mineralogy and Geochemistry Volume 63, Mineral Soc Amer, 399–426

Wenk H-R, Lutterotti L, Vogel S (2003) Texture analysis with the new HIPPO TOF diffractometer. Nucl Instrum Methods A 515:575–588

Wenk H-R, Lonardelli I, Vogel SC, Tullis J (2005) Dauphiné twinning as evidence for an impact origin of preferred orientation in quartzite: an example from Vredefort, South Africa. Geology 33:273–276

Wenk H-R, Lonardelli I, Rybacki E, Dresen G, Barton N, Franz H, Gonzalez G (2006) Dauphiné twinning and texture memory in polycrystalline quartz. Part 1: experimental deformation of novaculite. Phys Chem Minerals 33:667–676